Routing and photodetection in subwavelength plasmonic slot waveguides

Dany-Sebastien Ly-Gagnon[1,*], Krishna C. Balram[1], Justin S. White[2], Pierre Wahl[1,3], Mark L. Brongersma[2] and David A.B. Miller[1]

[1] Edward L. Ginzton Laboratory, Stanford University, Stanford, CA 94305-4088, USA,
e-mail: dalyx@stanford.edu, dalyx@alumni.stanford.edu
[2] Geballe Laboratory for Advanced Materials, Stanford University, 476 Lomita Mall, Stanford, CA 94305, USA
[3] Department of Applied Physics and Photonics, Free University of Brussels, Brussels 1050, Belgium

*Corresponding author

Abstract

The ability to manipulate light at deeply sub-wavelength scales opens a broad range of research possibilities and practical applications. In this paper, we go beyond recent demonstrations of active photonic devices coupled to planar plasmonic waveguides and demonstrate a photodetector linked to a two conductor metallic slot waveguide that supports a mode with a minute cross-sectional area of $\sim\lambda^2/100$. We demonstrate propagation lengths of $\sim10\lambda$ (at 850 nm), routing around 90° bends and integrated detection with a metal-semiconductor-metal (MSM) photodetector. We show polarization selective excitation of the slot mode and measure its propagation characteristics by studying the Fabry-Perot oscillations in the photo current spectra from the waveguide-coupled detector. Our results demonstrate the practicality of transferring one of the most successful microwave and RF waveguide technologies to the optical domain, opening up many opportunities in areas such as biosensing, information storage and communication.

Keywords: Photodetection; plasmonics; routing; waveguide.

1. Introduction

Metals have long been used to confine and manipulate radio-frequency and microwave signals on highly integrated and functional RF circuits [1, 2]. Transposing some of these concepts to the near-IR wavelength region could lead to highly functional optoelectronic circuits [3–7] with a tremendous impact in many important areas of nanotechnology such as nanoscale sources and detectors for future optical interconnects [8], heat-assisted magnetic recording (HAMR) for next generation hard drives [9], DNA sequencing [10], and many others where strong light matter interaction is required [11]. Such integrated optoelectronic circuits with nanoscale active components would require a flexible waveguiding platform to confine and route optical signals. Research in plasmonics

has been pursued by various groups for the light confinement that could be achieved with metals used in the backend processing of high volume silicon circuits [12]. While passive elements such as wavelength filters have been realized in various geometries [13, 14], active devices have primarily been coupled to planar metal-insulator-metal waveguides that support gap plasmons between two vertically stacked metal films [15–17]. This geometry provides sub-wavelength mode confinement in only one dimension (vertically). A platform that relies on a planar geometry to confine plasmons laterally and vertically [18] could provide true cross-section confinement, enable flexible routing of optical signal on a chip and facilitate the use of planar CMOS fabrication techniques to realize massively interconnected optical circuits which would be a part of future exascale systems.

In this paper, we unambiguously demonstrate guiding and routing of surface plasmon polaritons (SPP) in a deeply subwavelength mode and demonstrate active functionality with integrated detection using a metal-semiconductor-metal (MSM) photodetector. Our structures are analogous to the microwave slot line [1] and are fabricated with planar processing techniques comparable with current backend processing in CMOS. We demonstrate propagation lengths of $\sim10\lambda$ for guide cross-sections of $\sim\lambda^2/100$, and routing around 90° bends, clearly showing the controllable guiding of light at these length scales. We detect the plasmons by the photocurrent generated in an integrated silicon MSM detector located at the end of the guide. The coupling to nanoscale semiconductor structures enables the design of low capacitance, high speed on-chip photodetectors [19, 20] with active volumes approaching $\lambda^3/1000$. We extract the propagation characteristics of the mode by studying the Fabry-Perot spectra of the waveguide, which behaves as a low-Q resonator due to the weak reflection at the in-coupling point and the photodetector. To the best of our knowledge, this is the first time this measurement has been demonstrated for nanometer scale two-conductor coplanar plasmonic waveguides, and it shows that tight mode confinement preserves the Fabry-Perot fringes even in the presence of metallic loss. In addition, the measurements agree reasonably well with numerical simulations; this leads us to believe that the dielectric constants of metallic films do not change appreciably when patterned at the length scales discussed here and hence more complex structures can be reliably designed and modeled [21].

2. Device structure and fabrication of the waveguide-integrated photodetector

The structure of our device is shown in Figure 1A. The slot plasmon waveguide consists of two metal strips of 80 nm
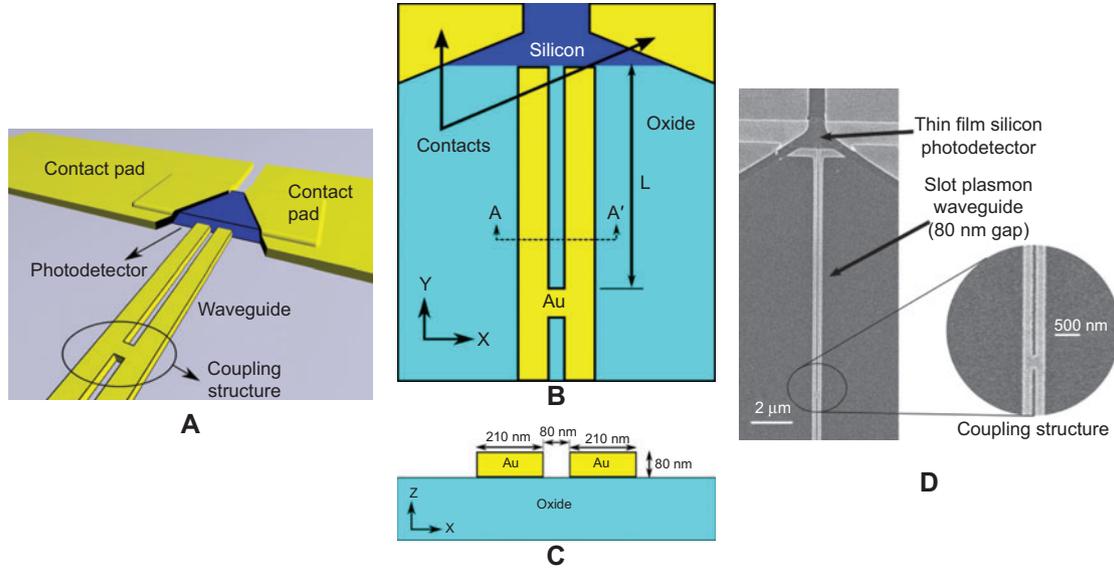
Figure 1 (A) Schematic of the device. (B) Plan view schematic of the device. (C) Cross-section of the waveguide A-A′. (D) SEM of the fabricated device with a magnified view of the coupling region.

thickness and 210 nm width, separated by 80 nm. The optical signal propagates in the 80 nm×80 nm slot region and is incident on an integrated silicon metal-semiconductor-metal (MSM) photodetector, which lies in the same plane as the waveguides. Figure 1B shows a plan view of the device, and Figure 1C shows a cross section of the waveguide. The silicon photodetector is used to convert highly confined slot plasmons with a free-space wavelength λ_0 between 800 nm and 1000 nm into an electrical signal. The coupling structure of the waveguide (where both conductors are connected together through a short circuit) acts both as a reflector and as a feed-in antenna.

We fabricated the plasmonic waveguide-integrated photodetectors from wafers of thin crystalline silicon films on silicon dioxide (referred to as oxide below). The starting material for the fabrication of the photodetectors was n-type silicon-on-insulator (SOI) wafers (1–5 ohm-cm) with a buried-oxide layer of 400 nm and a starting device (silicon) layer of 400 nm, which were repeatedly thermally oxidized at high temperature and etched in buffered hydrofluoric acid to partially consume the device layer such that the remaining device layer is 200 nm. The wafers were subsequently bonded to a Pyrex substrate and the silicon substrate (the "handle") of the SOI wafer was etched back, leaving a thin film of crystalline silicon on an oxide substrate. Mesa patterns were defined using standard optical lithography and tetramethylammonium hydroxide (TMAH) etchant. The electrical contacts were defined using standard optical lithography and lift-off of an e-beam evaporated metal film of Cr/Au/Cr (10/85/10 nm). Optical lithography and a standard lift-off procedure was then used to align to the bottom of the silicon mesa and define an e-beam evaporated metal film of 80 nm of Au (directly on the oxide) followed by 5 nm of Ti. Electron-beam lithography and argon-ion etching was then used to define the waveguide structures in this Au/Ti film. A scanning electron micrograph (SEM) of the fabricated structure is shown in Figure 1D.

We calculate the propagation constants of the waveguide structure shown in Figure 1C using COMSOL multiphysics. We assume a refractive index of n=1.44 for the oxide and use the refractive indices for gold as given by Palik [22]. In this geometry, the waveguides support only two modes, a slot plasmon mode which is mostly confined in the slot region between the two conductors (Figure 2A) and a strip plasmon mode which lies mostly beneath the two conductors (Figure 2B). In Figure 2A and 2B, the colors show the intensity (magnitude of the Poynting vector) in the y-direction, and the arrows indicate the direction and magnitude of tangential electric field (Ex and Ez). While the strip plasmon has a longer propagation length, its field profile is similar to the fundamental mode of a single metal strip without the slot region and its relatively weak confinement makes it less attractive for integration in opto-electronic devices. Figure 2C shows the calculated refractive indices and Figure 2D shows the propagation lengths for the slot plasmon and strip plasmon modes as a function of wavelength. The effective refractive index is given as $n_{eff}=Re(\gamma)/(2\pi/\lambda)$ where γ is the mode propagation constant and λ is the free-space wavelength. The propagation length is given as $1/Im(\gamma)$ and corresponds to the length before the field attenuates by a factor of $(1/e)$. The slot plasmon mode reaches a propagation length of 9 μm around a free space wavelength around 900 nm, which is more than 112 times the width of the slot where most of the optical energy is confined. In contrast, although the strip plasmon has a longer propagation length of 19 μm, it extends over more than the whole width of the pair of metal strips and to a substantial extent into the substrate also.

3. Excitation of the confined waveguide mode

We used finite-difference time-domain (FDTD) simulations [23] to explore the possibility of effectively coupling light
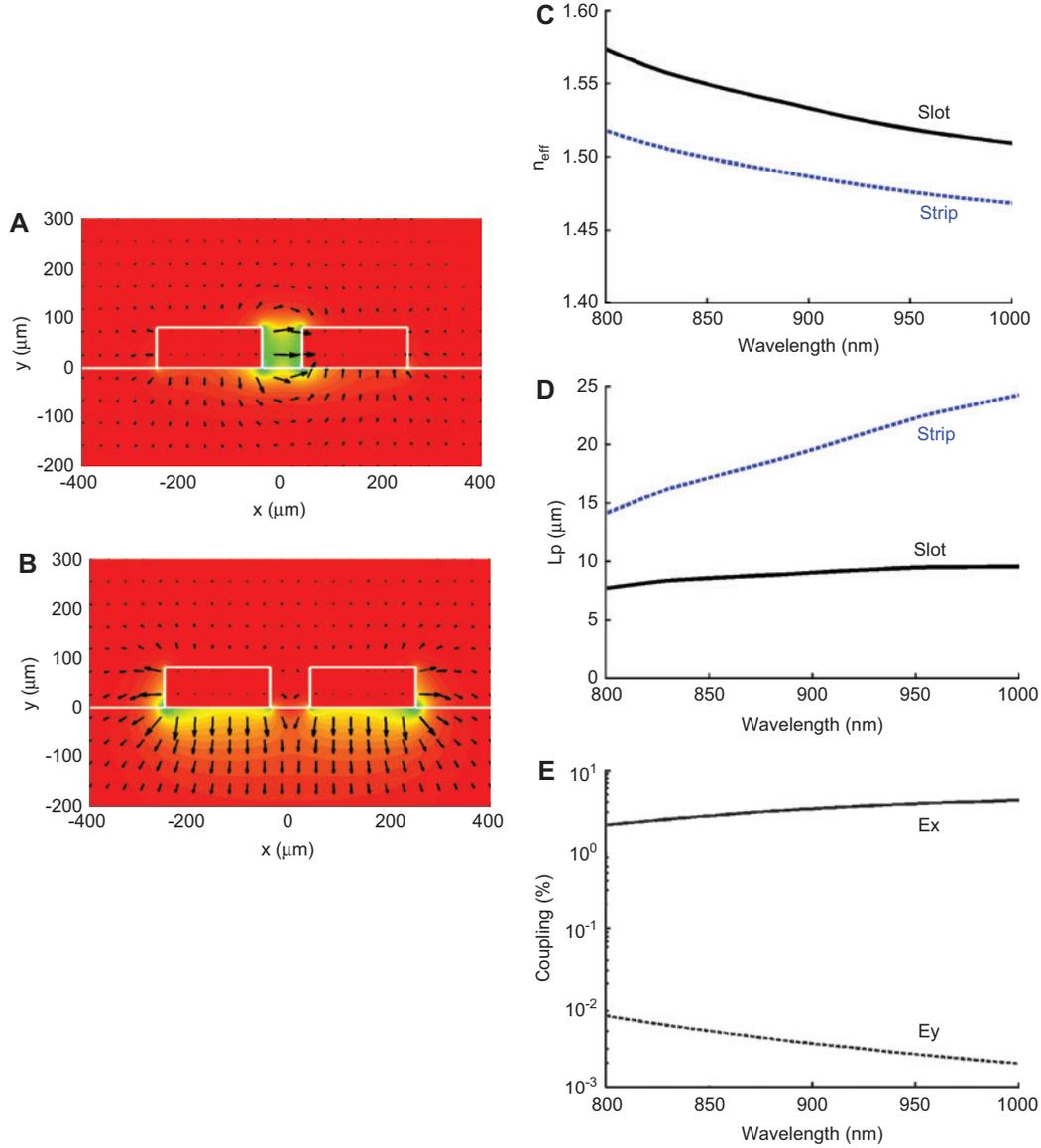
Figure 2 Mode and coupling simulations for the slot and strip plasmon mode. The substrate is oxide (n=1.44), the cladding is air (n=1) and the waveguide material is gold (with dielectric constant from Palik [22]). The dimensions of the waveguide are shown in Figure 1C. (A) Slot plasmon mode excited with x-polarized light at 900 nm. (B) Strip plasmon mode excited with y-polarized light at 900 nm. (C) Calculated effective refractive index for the slot (solid) and strip plasmon mode (dashed). (D) Propagation length for the slot (solid) and strip plasmon mode (dashed). (E) Coupling efficiency of a gaussian beam at the coupling structure with incidence in x-polarization (solid) and in y-polarization (dashed).

into the slot waveguide mode without coupling to the strip plasmon mode. The FDTD code is a custom code designed to perform FDTD simulations on a high-performance Graphical Processing Unit (GPU) [24]. When the coupling structure is top-illuminated with an incident Gaussian beam with its electric field polarized in the x-direction, the optical field couples to propagating slot plasmons that are launched away from the coupling structure. Our simulations show that the coupling with an x-polarized field (perpendicular to the waveguide direction) into the slot plasmon mode is more than 100 times more efficient than coupling with a y-polarized field (parallel to the waveguide direction) to the strip plasmon mode.

The coupling structure where coupling takes place is modeled as a shorted section of waveguide, where the slot is filled with metal throughout 400 nm of length in the propagation direction. In these simulations, the coupling structure is excited with a Gaussian beam from the air side. We calculate the coupling efficiency by integrating the power of a focused Gaussian beam at the coupling structure with FWHM of 1 μm in a 2 μm×2 μm area, which corresponds to more than a $4\lambda^2$ area at 900 nm, as the incident power. For the waveguide, gold is modeled as a 4-poles Lorentz material obtained by fitting the values from Palik in the 800–1000 nm wavelength range [22]. After propagating 5 μm in the waveguide, the power in the guide is integrated in an area of 2 μm×2 μm centered on the waveguide, and projected back to the coupling structure to take into account waveguide losses. This area contains more than 99.7% of the propagating Poynting vector in both the

slot plasmon mode and the strip plasmon mode at 900 nm. The coupling for the allowed modes is shown in Figure 2E. The coupling to the slot plasmon with incident field in the x-direction (Ex) is more than 2 orders of magnitude higher than the coupling to the strip plasmon with incident field in the y-direction (Ey), thus allowing us to selectively excite the strongly confined slot plasmon mode in this waveguide geometry.

The coupling of an x-polarized excitation to the strip plasmon is prohibited because of incompatibility in symmetry between the excitation polarization and the polarization of a guided strip plasmon mode. Conversely, a Gaussian beam polarized in the y-direction does not couple to the slot plasmon because of the polarizations are orthogonal. This structure can thus excite the slot plasmon without exciting the strip plasmon. We chose this coupling structure as the coupler to ensure that we were coupling only to the slot plasmon mode in our experiments, not for overall efficiency in coupling, which is ~1% for coupling to slot plasmons from a focused Gaussian spot, and we expect more efficient couplers could be devised at this wavelength.

We measured the photocurrent generated by the photodetector as a function of the position of the exciting laser spot to investigate the coupling and propagation in the highly-confined slot plasmon mode in these structures. A mode-locked Ti-Sapphire laser operating at 850 nm is chopped at a frequency of 1 kHz, attenuated to 150 μm and focused with a 20X microscope objective with numerical aperture of 0.4 onto the sample. The optical beam is held in a fixed position, while the sample position is controlled with an open-loop piezo-actuator stage with 50 nm step size. The photodetectors are held at a bias of 1V throughout the experiment and the signal is amplified with a SR870 preamp and monitored with a SR830 lock-in amplifier.

Figure 3A and 3B show the photocurrent maps as a function of the x-y position of the sample for an incident Gaussian beam polarized in the x- and y- direction, respectively. When the incoming electric field is polarized in the x-direction, we observe two distinguishable peaks. The larger peak corresponds to the optical beam being directly incident on the photodetector. The second peak, smaller in amplitude, appears only when the incident beam is polarized in the x-direction and at a position that corresponds to the beam being incident on the coupling structure. When the incident optical beam is polarized in the y-direction, we find that this second peak vanishes (as shown in Figure 3B). The measured contrast ratio between the signal in the two polarizations is >10x, but is limited by electrical noise.

We repeated these experiments on similar devices where the coupling structure was positioned at a different location in the waveguide. The results for line scans that intersect the middle of the photodetector are shown in Figure 3C. The signal amplitudes at 0 μm (where the input spot directly overlaps the detector) are generally similar in all cases. In each case, we observe two peaks when the incident beam is x-polarized, one corresponding to the direct illumination of the photodetector, and one corresponding to the location of the coupling structure in relation with the photodetector,

whereas we only observe a single peak when the incident beam is y-polarized. The ratio in photocurrent between direct illumination of the photodetector (large peak) and the magnitude of photocurrent with the light beam positioned over the coupling structure shows that the loss in the waveguide agrees with numerical calculations (see inset). We believe the deviations of the measured points from the straight line likely arise because the waveguide structure also behaves as a low-Q Fabry-Perot resonator (discussed in detail below), leading to an oscillatory modulation on what would otherwise be an exponential decay of the signal with guide length.

Further evidence of polarization dependence at the coupling structure, which corresponds to a selective excitation of the slot plasmon mode, can be observed in devices where the waveguide is routed through waveguide bends before being detected by the integrated photodetector. We measured the photocurrent as a function of position in x-polarization (Figure 4A) and in y-polarization (Figure 4B) for a device with a single 90° bends and a radius of curvature of 1.75 μm. Figure 4B shows the sharp increase in photocurrent when the incident beam is positioned at the coupling structure location. For a single bend, the y-polarization becomes the one that effectively couples to the slot plasmon, since the y-polarization is now oriented perpendicularly to the waveguide near the coupling structure. We repeated these measurements on a S-bend, formed by two 90° bends. In this structure, the x-polarization couples well, given the orientation of the coupling structure with respect to the incident polarization.

4. Formation of a low-Q resonator in the waveguide structure

The reflections at the photodetector as well as at the coupling structure can lead to the formation of a low-Q Fabry-Perot resonator within the waveguide structure. According to our simulations, reflections are sharply higher for the slot plasmon than for the strip plasmon. At the detector, the reflection coefficient for the slot plasmon reaches 35% at 850 nm, which is higher than the 5% reflection that the strip plasmon achieves at that wavelength. The high confinement of the slot plasmon thus leads to a higher reflection than we expect for the strip plasmon because of this mode mismatch. At the coupling structure, the situation is even more dramatic. More than 45% of the slot plasmon field is reflected across the entire wavelength range, while less than 3% of the strip plasmon field is reflected, suggesting that the slot plasmon could have enhanced interaction with a nanoscale volume of material that fills the slot.

The reflection at the end of the waveguide was calculated with FDTD. Full-field simulation results are shown in Figure 5A, with the magnitude of the Ex field shown for the slot mode and Ez for the strip mode at 900 nm, with incidence from the bottom of the plots. The amount of power that is reflected at the discontinuity is calculated by first integrating the power that goes through a cross-section located 2 μm before the discontinuity, and the result is substracted from the amount of power integrated over the same cross section in a calibration
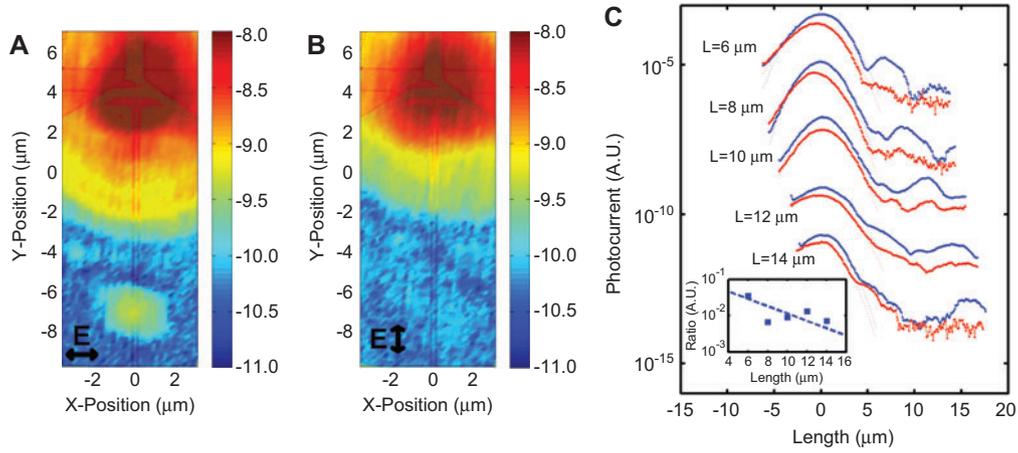
Figure 3 (A and B) Measured photocurrent (log scale) vs. X-Y position of sample for x-polarized (A) and y-polarized (B) incidence on a 10.5 μm waveguide with overlayed SEM. (C) Photocurrent (log scale) vs. Y position for x-polarized (blue) and y-polarized (red) light for a light beam centered over the waveguide in the X direction. Inset shows the ratio of photocurrent when measured at the coupling structure with respect to direct incidence on the photodetector and a line with a slope corresponding to the simulated attenuation length (dashed). The curves have been displaced vertically for clarity.

simulation without the discontinuity. The calculated reflected power is then normalized to take into account waveguide losses.

The results are shown in Figure 5B for the wavelength range under investigation. When the field is confined in the slot mode, more than 70% of the field is reflected at an open-ended waveguide. This can be explained by the high confinement of the field and low overlap with free-space modes, which provides poor coupling to propagating free-space modes. In comparison, reflections for the strip mode
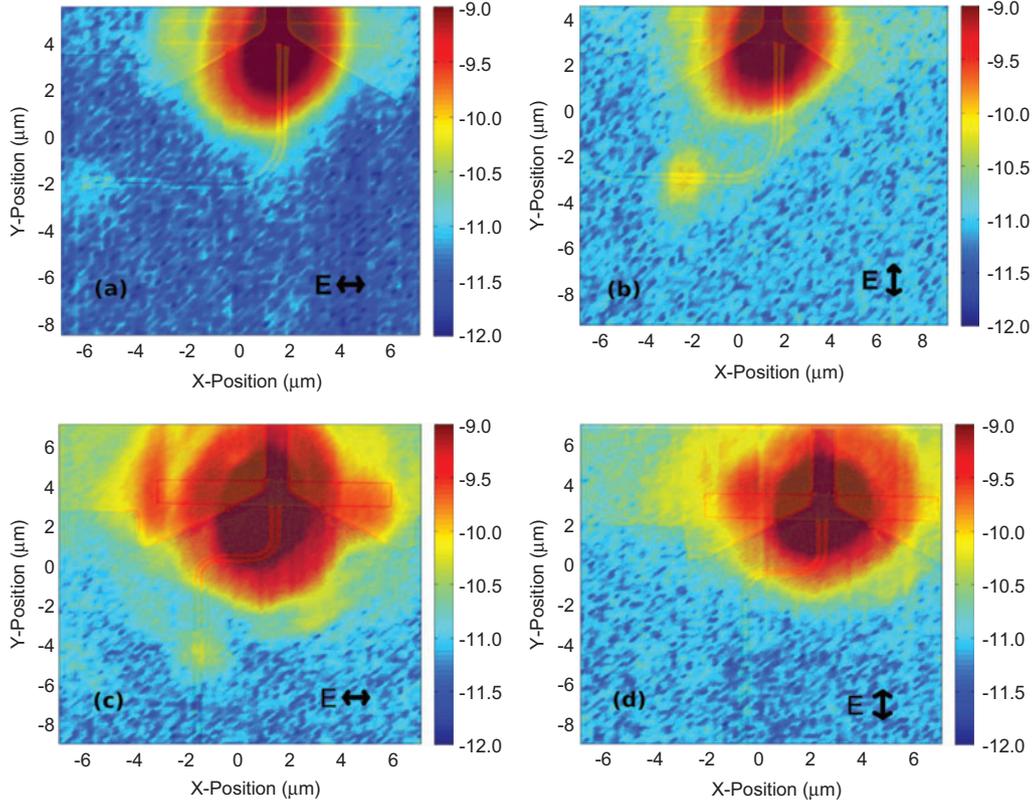

Figure 4 (a–d) Measured photocurrent (log scale) vs. X-Y position for 90° bends. (a) and (b) show results for a single 90° bend for light incident in (a) x-polarization and (b) y-polarization. Similarly, (c) and (d) show the results for a S-bend (two 90° bends). SEM pictures of the devices are overlayed.
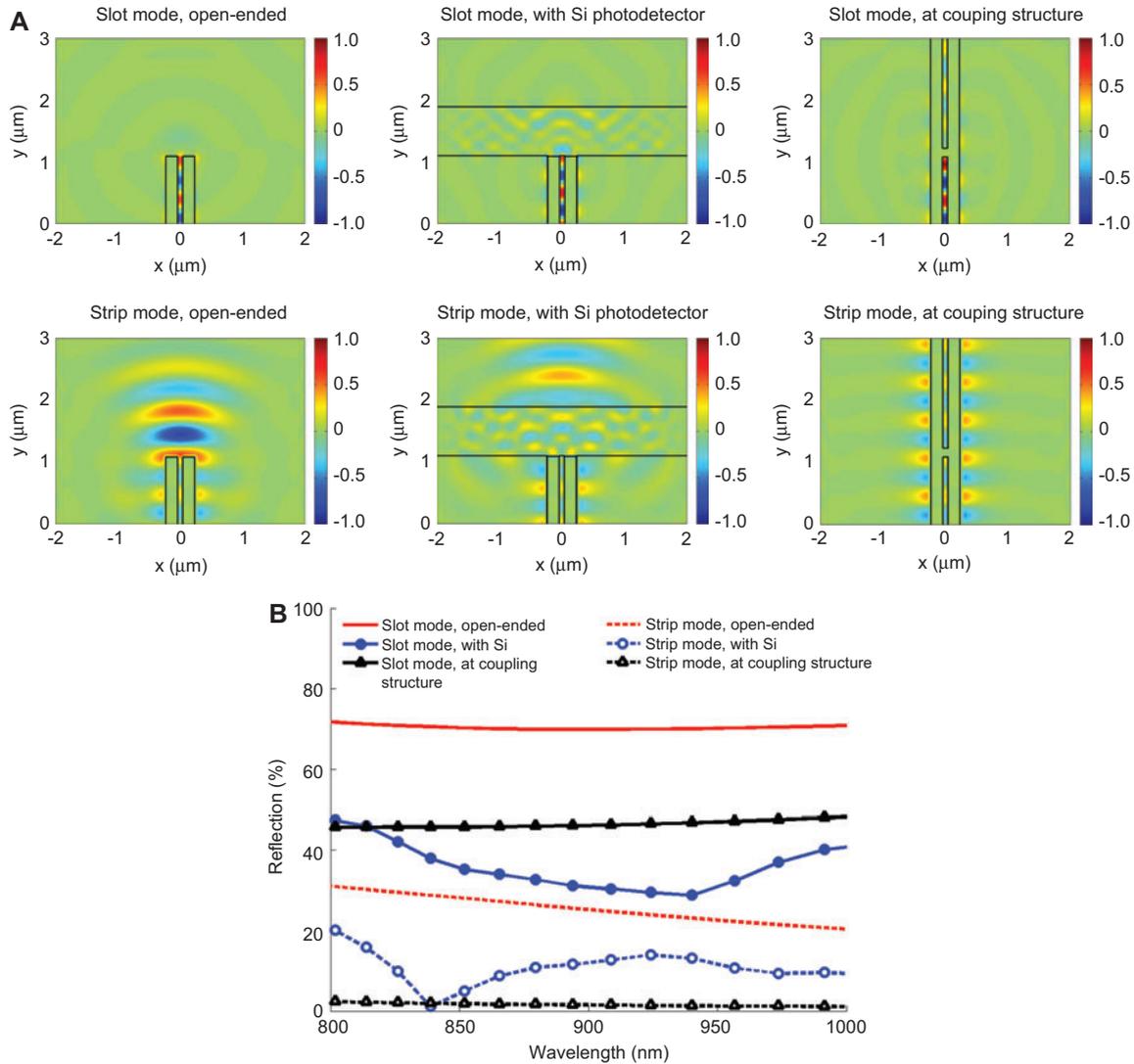
Figure 5 Field simulations of the reflection of the slot and strip plasmon modes at the end of the waveguide. The dimensions of the waveguide are shown in Figure 1C, with air as cladding (n=1), oxide as substrate (n=1.44), and gold as the waveguide material (dielectric constants from Palik [22]). The waveguide is either open-ended, terminated by a Si photodetector, or with the coupling structure. (A) Field simulations showing reflections in the structure at the end of the waveguide at 900 nm wavelength for each of the cases, for both the slot and the strip plasmon mode. Field plots on the upper pane show the Ex-field while those in the lower pane show the Ez-field. (B) Reflected power from the waveguide at different interfaces.

are below 30%, indicating that the strip mode can more easily be matched to propagating free-space modes. A similar effect is observed when a detector is present at the end of the waveguide. Although reflections are slightly lower in the presence of the detector element (which has a high refractive index), the slot plasmon mode is more effectively reflected from the detector than the strip plasmon mode.

The simulations also indicate that the presence of the coupling structure has a very significant effect for the reflection of the slot plasmon mode. The slot plasmon reflection coefficient at the detector is lower than for the case where the slot plasmon reaches an open-ended waveguide (70%). This difference in reflectivities for the slot plasmon can be explained by noting the difference in modal size in free space and in a large dielectric constant material, in this case silicon. The field

is effectively reflected from the coupling structure, as can be seen from the field amplitudes in Figure 5A. The difference in reflection between the slot mode and the strip mode incident upon the coupling structure is very large, which is consistent with the slot mode having most of its energy confined in the slot region. The strip mode does not interact strongly with the coupling structure, and the reflection coefficient is below 2% across this wavelength range.

We experimentally demonstrated the effect of multiple reflections effect in a low-Q cavity formed between the coupling structure and the detector in the measured photocurrent. By exciting the waveguide at the coupling structure, we monitored the photocurrent as we tuned the incident wavelength of the laser. The results are shown in Figure 6 for an 8.5 μm length cavity, where we normalized the collected photocurrent
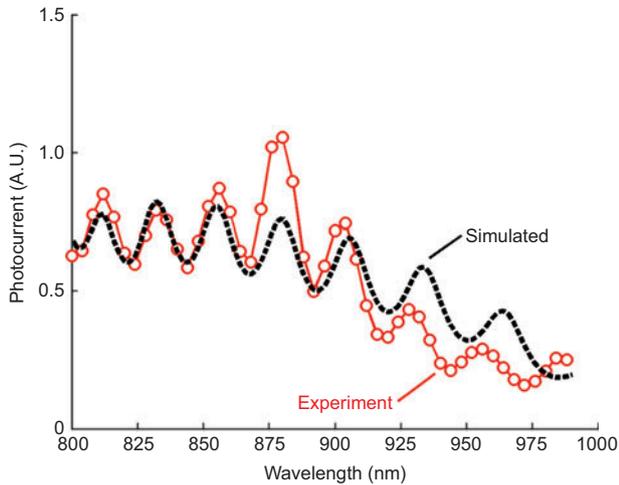
Figure 6 Measured device responsivity (solid) and simulated responsivity (dashed) for an 8.5 μm long waveguide, showing Fabry-Perot fringes.

with respect to the incident power. Our experimental results show the formation of Fabry-Perot fringes, where the fringe spacing and fringe depth is consistent with what we expect from the numerically calculated mode indices, waveguide losses, reflection coefficients and finite absorption in the semiconductor photodetector.

The spacing that we observe between the peaks corresponds well to the expected fringe spacing, and is strongly influenced by the length and the effective refractive index of the mode. The values we obtain from our experiments are consistent with the physical cavity length measured by SEM and the numerically calculated effective mode index of 1.55. The ratio between the maximum and minimum values around a peak is dependent on the cavity length, the waveguide losses and the reflection losses at the silicon and at the coupling structure. Assuming the numerically calculated values for reflection, we can estimate the propagation length with this ratio. From our measurements, we estimate a field propagation length of 9.5 μm around 850 nm, which is very close to the 8.7 μm that we obtain from simulations. In comparison, the reflections at the coupling structure for the strip plasmon mode are very weak, and would thus not lead to such pronounced spectral features. The comparison of the fringe depth to simulations thus provides a reliable estimate for the propagation loss of the slot plasmon mode, and we find that despite fabrication imperfections, the slot plasmon mode shows propagation and reflections that are close to those expected from simulations. On the other hand, since reflections for the strip plasmon mode are much lower, we would expect a much smaller fringe depth for that mode.

5. Conclusions

Our results directly show that plasmonic slot waveguides are a viable approach for guiding light at both multiple-micron and submicron scales and concentrating into deeply subwavelength

semiconductor photodetector volumes. Performance agrees well with simulations, allowing such guides to be predictably designed. These guides could have various uses in sub-wavelength optoelectronic systems: they could allow deeply sub-micron sized photodetectors to be positioned extremely close to transistors for minimized receiver capacitance [8] by transporting light from other optical layers or from antennas or antenna arrays; they offer optical impedance matching of detectors for greater efficiency [20], and, when combined with light or plasmon sources, they could permit efficient short-distance optical interconnects. The tight light concentration in such guides also suggests combining such guides with quantum-confined structures such as quantum dots and optically-active molecules. Due to their planar geometry, we can envisage that two-conductor plasmonic waveguides integrated with optoelectronic devices could offer a platform for functional subwavelength optoelectronic circuits that is similar to microwave stripline circuits in conventional radio-frequency electronics, opening a new generation in optoelectronic systems.

Acknowledgements

References

[1] Pozar DM. Microwave engineering. Wiley, 2011.

[2] Ramo S, Whinnery JR, Van Duzer T. Fields and waves in communication electronics. Wiley, 1994.

[3] Engheta N. Circuits with light at nanoscales: optical nanocircuits inspired by metamaterials. Science 2007;317(5845):1698–702.

[4] Schuller JA, Barnard ES, Cai W, Jun YC, White JS, Brongersma ML. Plasmonics for extreme light concentration and manipulations. Nature Mat 2010;9:193–204.

[5] Gramotnev DK, Bozhevolnyi SI. Plasmonics beyond the diffraction limit. Nature Photon 2010;4:83–91.

[6] Stehle C, Bender H, Zimmermann C, Kern D, Fleischer M, Slama S. Plasmonically tailored micropotentials for ultracold atoms. Nature Photon 2011;5:494–8.

[7] Atwater HA, Polman A. Plasmonics for improved photovoltaic devices. Nature Mat 2010;9:205–13.

[8] Miller DAB. Device requirements for optical interconnects to silicon chips. Proc IEEE 2009;97(7):1166–85.

[9] Kryder MH, Gage EC, McDaniel TW, Challener WA, Rottmayer RE, Ju G, Hsia Y-T, Erden MF. Heat assisted magnetic recording. Proc IEEE 2008;96(11):1810–35.

[10] Eid J, Fehr A, Gray J, Luong K, Lyle J, Otto G, Peluso P, Rank D, Baybayan P, Bettman B, Bibillo A, Bjornson K, Chaudhuri B, Christians F, Cicero R, Clark S, Dalal R, deWinter A, Dixon J, Foquet M, Gaertner A, Hardenbol P, Heiner C, Hester K, Holden D, Kearns G, Kong X, Kuse R, Lacroix Y, Lin S, Lundquist P, Ma C, Marks P, Maxham M, Murphy D, Park I, Pham T, Phillips M, Roy J, Sebra R, Shen G, Sorenson J, Tomaney A, Travers K, Trulson M, Vieceli J, Wegener J, Wu D, Yang A, Zaccarin D, Zhao P, Zhong F, Korlach J, Turner S. Real-time DNA sequencing from single polymerase molecules. Science 2009;323:133–8.

[11] Chang DE, Sorensen AS, Demler EA, Lukin MD. A single-photon transistor using nanoscale surface plasmons. Nature Phys 2007;3:807–12.

[12] Ozbay E. Plasmonics: merging photonics and electronics at nanoscale dimensions. Science 2006;311:189–93.

[13] Bozhevolnyi SI, Volkov VS, Devaux E, Laluet J-Y, Ebbesen TW. Channel plasmon subwavelength waveguide components including interferometers and ring resonators. Nature 2006;440:508–11.

[14] Han Z, Forsberg E, He S. Surface plasmon bragg gratings formed in metal-insulator-metal waveguides. IEEE Phot Tech Lett 2007;19(2):91–3.

[15] Neutens P, Van Dorpe P, De Vlaminck I, Lagae L, Borghs G. Electrical detection of confined gap plasmons in metal–insulator–metal waveguides. Nature Photon 2009;3: 283–6.

[16] Walters RJ, van Loon RVA, Brunets I, Schmitz J, Polman A. A silicon-based electrical source of surface plasmon polaritons. Nature Mat 2009;9:21–5.

[17] Dionne JA, Diest K, Sweatlock LA, Atwater HA. PlasMOStor: a metal-oxide-Si field effect plasmonic modulator. Nano Lett 2009;9(2):897–902.

[18] Veronis G, Fan S. Modes of subwavelength plasmonic slot waveguides. J Lightw Technol 2007;25:2511–21.

[19] Tang L. Nanometre-scale germanium photodetector enhanced by a near-infrared dipole antenna. Nature Photon 2008;2:226–9.

[20] Ly-Gagnon DS, Kocabas SE, Miller DAB. Characteristic impedance model for plasmonic metal slot waveguides. IEEE J Sel Topics Quantum Electron 2008;14(6):1473–8.

[21] Feigenbaum E, Atwater HA. Resonant guided wave networks. Phys Rev Lett 2010;104(14):147402–5.

[22] Palik ED. Handbook of optical constants of solids. NewYork: Academic, 1985.

[23] Taflove A, Hagness SC. Computational electrodynamics: the finite-difference time-domain method. Third Edition (Artech House Publishers, 2005).

[24] Wahl P, Ly-Gagnon DS, Debaes C, Miller DAB, Thienpont H. NUSOD'11, Paper MB2, Rome, Italy, September 5–8, 2011.